SPECTROSCOPIC STUDY OF THE LASER PRODUCED DYSPROSIUM PLASMAS

DAMIR VEŽA AND SLOBODAN MILOŠEVIĆ

Institute of Physics, P.O.Box 304, HR-10001 Zagreb, Croatia

**This paper is dedicated to Professor A. Bonefačić on the occasion
of his 70th birthday**

We report the observations of the excimer laser-induced dysprosium plasma. The time evolution of DyI and DyII selected resonance line intensities and line widths was studied. It is found that the time development of the plasma plume can be significantly influenced by the presence of argon backing gas. The comparison of the measurements of dysprosium atomic line widths made in vacuum and in argon shows a small influence of argon on the measured Stark line widths.

1. Introduction

Current interest in the spectroscopy of rare earth elements has been induced by the recent parity and time-reversal experiments [1], the need for a more accurate determination of the density of rare earth elements in stellar atmospheres [2,3], and the importance of rare earths in the physics and technology of lighting devices [4]. The dysprosium metal is a typical member of rare-earth elements family, which appears to be spectroscopically interesting in all encountered cases. However, the data on Stark broadening of dysprosium lines are not reported in literature, yet [5]. A few recent papers on the spectroscopy of DyI, DyII and DyIII are focussed on the measurements of gf-factors [6], lifetime measurements [7], isotope shifts and hyperfine structure [8], and accurate line positions of different spectrally important series of lines [9].

The lack of Stark broadening measurements among spectroscopic experiments investigating dysprosium is caused by specific experimental difficulties. This metal has a high melting temperature ($T_m \approx 1680$ K) and its vapor is very corrosive [10]. To obtain high enough density of neutral atoms, a significantly higher temperature must be reached. This precludes the use of a standard laboratory approach like stainless-steel heat-pipe technology. The atomic beam technique [11] or sputtering discharge [12] do not supply high enough density of electrons, ions and atoms for broadening observations. However, there are two promising ways to obtain a high plasma density and to study the plasma broadening effects. First solution could be a high-pressure discharge burner made of alumina and filled with Ar as a starting gas and Dy-Hg amalgam [13]. Alternatively, a burner made of quartz, filled with Ar as a starting gas and a Dy-based metal halide can be used [13]. A disadvantage of the discharge-based technique is that a multicomponent plasma must be studied. However, a study of a multicomponent Dy-Hg-Ar plasma is an important task for itself, because it is the main constituent of a high-pressure metal-halide discharge lamp [4]. Second solution can be the use of a powerful pulsed laser producing a time-dependent high density plasma plume by simple ablation of a dysprosium target. The usefulness of this technique for investigation of Stark broadening of lithium atomic lines at high electron densities has been recently demonstrated [14]. In this work we report the results of a preliminary experiment where excimer laser ablation of metallic dysprosium was used for plasma production and studies of the time evolution of DyI $6s^2\ ^1S_0 \longleftarrow 6s6p\ ^1P_J^0$ and DyII $6s\ ^2S_{1/2} \longleftarrow 6p\ ^2P_J$ resonance line fluorescence.

2. *Experimental details*

The experimental apparatus is shown in Fig. 1. The whole experimental set-up consisted of a chamber with a rotating Dy-metal target, an excimer laser, a 0.6 m monochromator equipped with a 1200 g/mm grating, a photomultiplier for the detection of plasma fluorescence, a box-car averager, and an A/D converter for the computer acquisition of the fluorescence signal.

The Dy target was placed in a vacuum-tight chamber evacuated by means of a roots pump system. Before use, the metal surface was polished with a fine polishing paper and washed in alcohol. The measurements were made either in vacuum (better than 10^{-3} mbar) or in argon atmosphere. In the latter case, the high-purity argon (at pressures up to 100 mbar) was used as a backing gas. An excimer laser operating at 308 nm was used for ablation of Dy samples. The laser pulse duration was about 20 ns (FWHM), laser repetition rate was fixed at 5 Hz, and the maximum pulse energy measured in front of the vacuum chamber entrance window was about 25 mJ. The central uniform part of the laser beam was isolated by an aperture and focussed by a spherical quartz lens of 300 mm focal length (diameter: 40 mm). The laser beam focussed to a waist of about 20 μm, hit the Dy-surface at normal incidence. The fluence of the laser beam was varied by calibrated quartz plates of different thickness put into the laser beam.
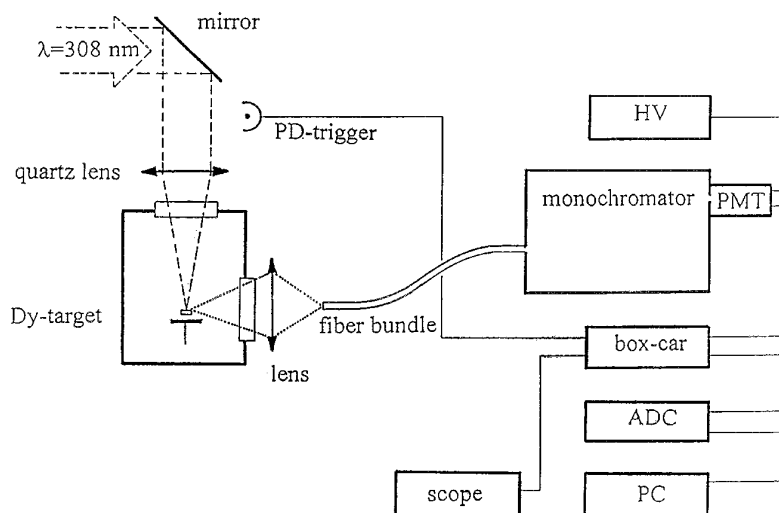
Fig. 1. Experimental arrangement for laser ablation and measurement of the Dy-plume emission.

The relative sensitivity of our detection system and the resolution power of our monochromator have been determined independently, before fluorescence measurements. The overall detection system sensitivity was measured using a standard tungsten ribbon lamp. The resolution of the monochromator can be varied by changing the width of the entrance and the exit slits. We have found that 20 μm wide monochromator slits are an optimal choice to obtain a high throughput and a high resolution power. The monochromator resolution was determined using a HeNe laser and observing the diffused light of the laser line at 632.8 nm. Typically, the 20 μm wide entrance and exit slits produce a pure triangular instrumental profile with the 0.045 nm FWHM.

Optical emission of the laser-generated plume was monitored parallel to the rotating Dy-target surface. The rotating target ensures an even wear of the Dy surface, and prevents "sinking" of Dy plume into the crater caused by etching action of subsequent laser pulses. The fluorescence of the plasma plume obtained by laser ablation was not spatially analyzed at this stage of our experiment. The fluorescence was collected with a large aperture lens, and the fluorescence spot was imaged onto the entrance slit of the monochromator via a large diameter optical fiber bundle. The bundle exit facet was fixed to the entrance slit of the monochromator. The dispersed light was detected by a blue-sensitive photomultiplier and the photocurrent was fed into a box-car averager, an AD/DA converter, and stored in a personal computer for further processing. The signal for the triggering of the box-car averager was obtained from a fast photodiode monitoring a small part of the laser beam.

3. Results and discussion

We studied general spectral features of laser generated plasma plume (in vacuum and in argon backing gas): the energy threshold for the plasma formation, the time evolution of resonance line intensities, the time evolution of neutral and ion line-widths, and the conditions to detect the impurities (according to the manufacturer declaration the sample is 99.9% pure Dy containing 0.1% Ho and Y as impurities [15]).
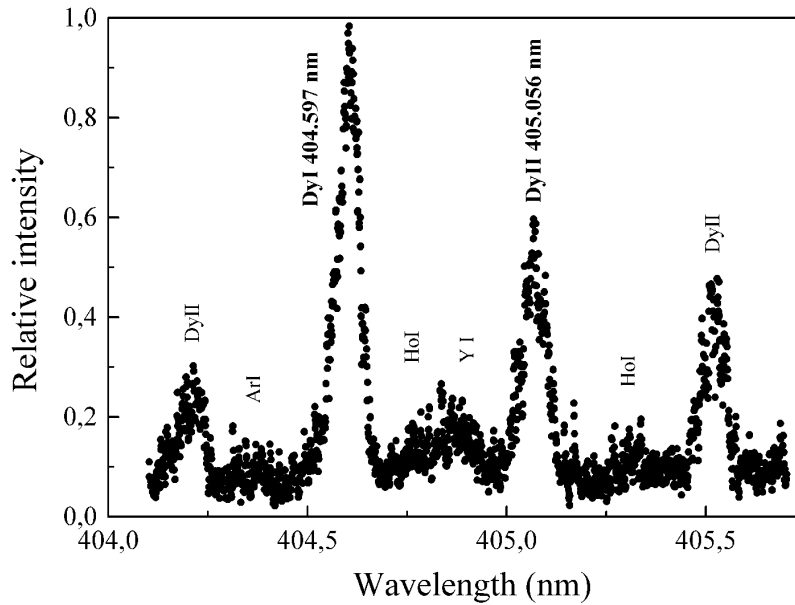

Fig. 2. Characteristic part of emission spectrum of dysprosium plasma plume. The spectrum represents the fluorescence induced by excimer laser pulses in vacuum, using the 400 ns delay after the laser pulse, and 100 ns gate width.

The spectrum of atomic and ionized dysprosium is a very complex one [16,17], with many strong resonance lines and hundreds of weaker lines originating in transitions between excited states. Even with the computer data acquisition and later numerical analysis of digitally recorded spectra, the analysis of such a spectrum is a rather demanding and time-consuming task. Therefore, we have chosen for the analysis a small part of the spectrum containing resonance lines of atomic and ionic dysprosium. Figure 2 represents this section of the dysprosium plasma plume spectrum, showing several DyI and DyII lines and atomic lines of both impurity elements. In this small spectral range, the system spectral response is almost flat. The identification of spectral lines appearing in the plume spectrum has been performed using the standard tables of atomic energy levels, wavelengths and transition probabilities [16]. A simplified dysprosium term-diagram showing the origin of the resonance lines of atomic and ionized dysprosium is given in Fig. 3. The ground state of dysprosium atom has the configuration $4f^{10}(6s^2\ ^5I_8)\ ^1S_0$ and the first excited state has the configuration $4f^{10}(6s6p\ ^5I_{Ji})\ ^{1,3}P^0_{Jp}$ [17]. The strong transitions

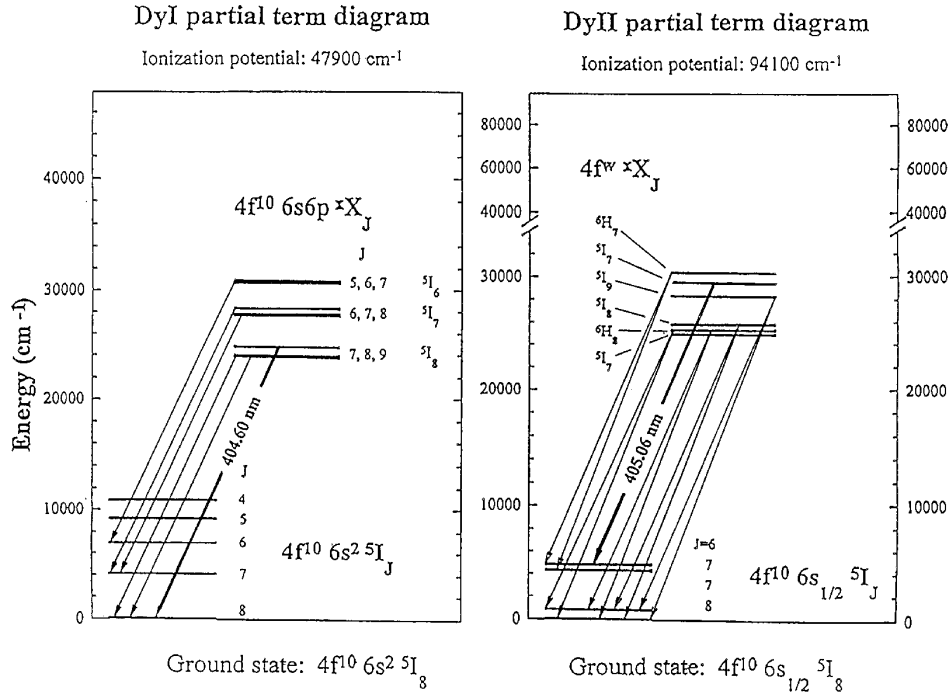*Fig. 3. Partial term diagram of* DyI *and* DyII, *showing ionic and atomic emission lines measured in this experiment. Ground state of* DyI *is* $4f^{10}(^5I_J)(6s^2\ ^1S_0)$ *and first excited states have configuration* $4f^{10}(^5I_{Ji})(6s6p\ ^{1,3}P^0_{J2})J'$. *Ground state of* DyII *is* $4f^{10}\ (^5I_8)\ 6s_{1/2}$ *and first excited states have configuration* $4f^w\ (^xI_{Ji}\ or\ ^xH_{Ji})\ 6p$.

are limited solely to the $6s^2\ ^1S_0 \longleftarrow 6s6p\ ^1P^0_{Jp}$ array. In all transitions observed in this experiment, there is no change of the core quantum numbers $\alpha_1L_1S_1J_1$. Thus, for a given $\alpha_1L_1S_1J_1$, there are three strong dipole-allowed lines corresponding to $\{J=J_1\} \longleftarrow \{J' = J_1, J_1 \pm 1\}$ transitions. The lines corresponding to transitions from the $6s6p\ ^3P_J$ levels and/or to a change in core quantum numbers $\alpha_1L_1S_1J_1$ are significantly weaker. Dysprosium ion has the ground state configuration $4f^{10}\ (6s\ ^5I_8)\ ^2S_{1/2}$ and the first excited states have $4f^w(6p\ ^5I_{Ji})\ ^2P_{Jp}$ configuration. The strong transitions belong to the array $6s\ ^2S_{1/2} \longleftarrow 6p$ $^2P_{0;1/2,3/2}$ for which $\alpha_1L_1S_1J_1$ does not change. The strong lines are more numerous than in the neutral-atom example because one can have an array of lines corresponding to any of the dipole-allowed $\{J=J_1 \pm 1/2\} \longleftarrow \{J' =J_1 \pm 1/2, J_1 \pm 3/2\}$ transitions. In this experiment, we were focussed to the observation of neighboring resonance lines of DyI $(6s^2\ ^1S_0\ (J=8)$ $\longleftarrow 6s6p\ ^1P^0_J\ (J=7)$ at 404.597 nm), and DyII $(6s\ ^2S_{1/2}\ (J=6) \longleftarrow 6p\ ^2P_J\ (J=7)$ at 405.056 nm).
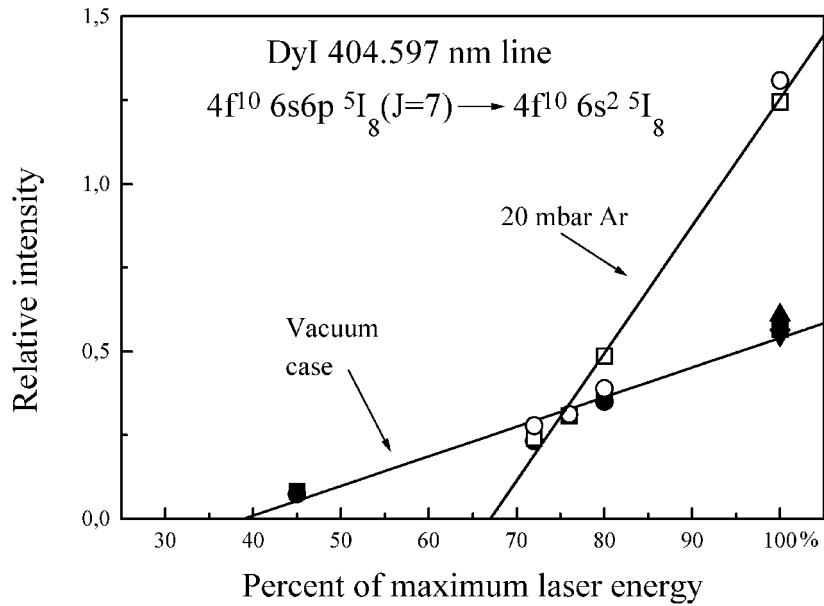
Fig. 4. Determination of the threshold energy for ablation in vacuum (solid symbols) and in argon (open symbols). Maximum pulse energy was 25 mJ. *Maximum pulse energy was 25* mJ, *and the laser spot size was 1* mm×0.3 mm. *Laser beam was focussed by a 300* mm *focal length quartz lens.*

In the first part of our experiment, we investigated the threshold for the plasma formation in vacuum and in argon backing gas. The integral intensity (the area under the spectral line) of the DyI 404.597 nm line was measured for different laser fluences. When ablation has been induced in argon, a higher threshold for plasma breakdown has been measured. A least-square linear fit procedure gives the threshold for the plasma formation in both cases (see Fig. 4). The threshold for the plasma breakdown is lower in the vacuum case, but the line intensities increase much faster with the increase of laser fluence if ablation has been induced in argon. This can be explained by examining the role of argon buffer gas in plasma creation [18]. If a pulsed laser beam irradiates the dysprosium surface in vacuum, the illuminated area (within the beam waist) is heated depending on the absorption coefficient of dysprosium metal. The absorbed energy causes the local increase of the surface temperature, leading to the melting of the target area. Melted metal evaporates in the form of clusters, molecules and atoms. The evaporated dysprosium atoms can be ionized in a two-photon ionization process by excimer laser photons (the excimer laser photon energy is 32467 cm^{-1}, and DyI ionization potential is 47900 cm^{-1}). The two-photon ionization of DyI is a source of seed electrons in dysprosium vapor. In addition, because of high surface temperature, some seed electrons can be emitted by surface thermionic emission, too. The seed electrons are very important in plasma breakdown and plasma heating process. They gain energy by the inverse bremsstrahlung process, which is the main mechanism of absorption of laser radiation in the dysprosium vapor [18]. During this process, seed free

electrons became more and more energetic and finally became able to ionize neutral vapor atoms, inducing an avalanche plasma breakdown. If the plasma ablation process has been induced in an argon atmosphere, the process of melting, evaporation, seed electron production and plasma initiation is accompanied by simultaneous plasma heating and breakdown in a thin argon layer in a close contact with the melted dysprosium spot. Thus, the laser radiation heats not only the metal surface but indirectly the argon buffer gas, too. This may explain a higher threshold for plasma formation in argon. When laser fluence is over the threshold level, the hot argon-dysprosium plasma mixture is more efficient in collisional excitation of dysprosium atoms and ions, producing stronger spectral lines compared to the vacuum case.
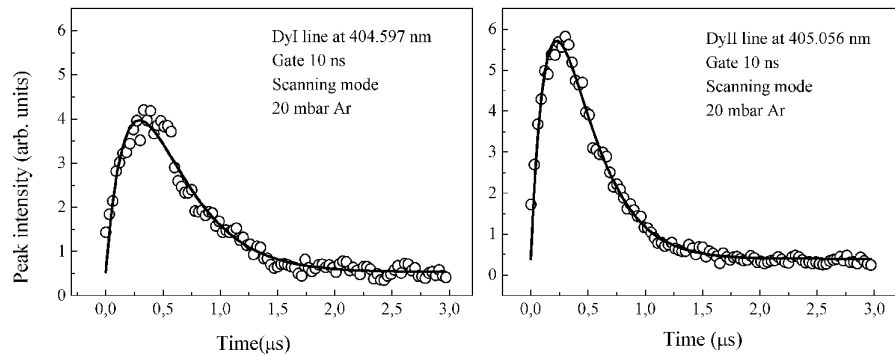

Fig. 5. An example of the time evolution of dysprosium plasma emission.

In the second part of our experiment, we studied the influence of argon on the plasma dynamics. We used the ionic line at 405.056 nm and the atomic line at 404.597 nm for this analysis. The intensity at the peak of atomic and ionic line has been measured vs. time delay after the laser pulse, measuring the evolution of ionic and atomic fluorescence at fixed argon pressures from 10 to 100 mbar. An example of time-dependence of the peak line intensity of the atomic and the ionic resonance lines at 20 mbar Ar is shown in Fig. 5. The maximum of both, ionic and atomic line intensities, is reached about 300 ns after the laser pulse. There is a certain delay between ionic and atomic fluorescence, and the proper analysis of such time-dependent signals can give us the information on the evolution of ionic and atomic component of the plasma. The simplified excitation/deexcitation scheme valid for the ionic and the atomic component of the plasma is given in Fig. 6. The leading edge of the laser pulse creates a dense, fast-decaying pool of the mixture of dysprosium atoms and ions in the first and, probably, the second ionization stage. In this stage, the ions dominate in the plasma because of the high plasma temperature and the high electron density [18]. This plasma decays within tens of nanoseconds to the plasma state where singly ionized dysprosium ions dominate, and subsequently to more neutral dysprosium plasma/vapor mixture. The upper level of monitored DyII (and DyI) line denoted by N_u is populated by different collisional and radiative channels during the decay of the initial pool of dysprosium ions. The total effective probability of population of the upper ionic (and atomic) level N_u is denoted by Γ_{pu}. The upper state decays by spontaneous emission (Γ_{ue})
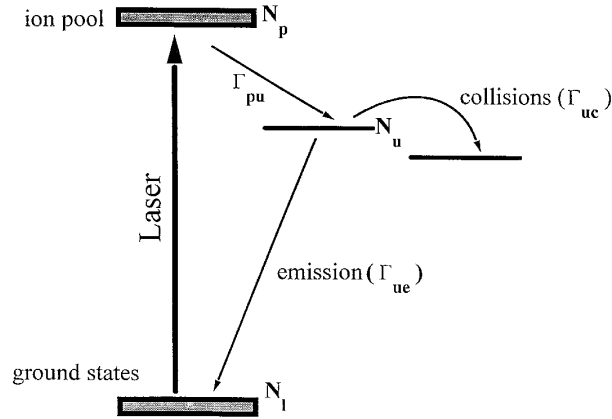
Fig. 6. Simplified excitation/deexcitation scheme for dysprosium plasma evolution after excitation by an excimer laser pulse.

and in collisions with neighboring particles (Γ_{uc}), and the total effective decay constant of this level is $\Gamma_u = \Gamma_{uc} + \Gamma_{ue}$. The rate equation describing the time evolution of ionic (and subsequently atomic) population in the radiating level N_u can be written as

$$\frac{dN_u}{dt} = N_p(t)\Gamma_{pu} - N_u(t)\Gamma_u, \tag{1}$$

where N_p designates the density of the pool of all ions and atoms contributing to the population of particles in the radiating state N_u at the time instant t, by ionization, decay, radiation and other processes. The solution of this differential equation is a double exponential form dependent on an effective population time τ_p and an effective decay time τ_u:

$$N_u(t) = N_{p0}\frac{\tau_u}{\tau_u - \tau_p}(e^{-t/\tau_u} - e^{-t/\tau_p}), \tag{2}$$

where

$$N_p(t) = N_{p0}e^{-t/\tau_P}. \tag{3}$$

The initial conditions are

$$N_u(0) = 0 \quad \text{and} \quad N_{p0}(0) = 0, \tag{4}$$

where N_{p0} designates the density of all ions and atoms contributing to the population of ions or atoms in the radiating state N_u, by radiation, decay and other processes. The result of such an analysis for ionic and atomic resonance line is given in Fig. 7, showing the influence of the argon backing gas to the population and radiation dynamics of an ionic (6p ^{2}P, $J = 7$) and an atomic (6s6p ^{1}P^0, $J = 7$) resonance state in dysprosium. In the absence of argon, the effective population times of ionic and atomic levels are the same. When

ablation is induced in the argon atmosphere, the (ionic and atomic) effective population times τ_p of the resonance
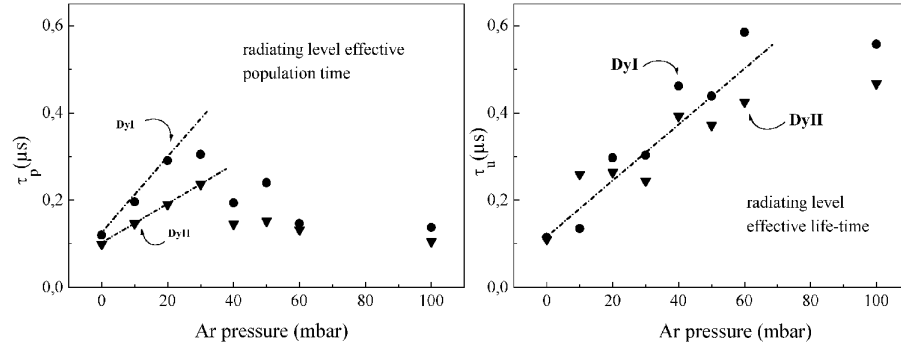

Fig. 7. Dependence of effective population times τ_p and effective level life-times τ_u for resonance states of DyI and DyII.

level N_u rise linearly up to 40 mbar of Ar pressure. At higher argon pressures, τ_p saturates at a value of about 0.1 μs. It is important to note that the ionic process is faster than the atomic one: at the same Ar pressure, the effective population time for the upper level of the atomic line is about 50% slower. On the contrary, the effective level decay time τ_u of the ionic (and atomic) resonance level are identical, and increase linearly with Ar pressure up to 40 mbar. The τ_u tends to a constant effective lifetime of about 0,5 μs at higher argon pressures. This behavior is reasonable and consistent with the excitation/deexcitation scheme shown in Fig. 6 and the model given by Eqs.(1-4). The subsequent decay of dysprosium plasma first gives rise to the appearance of singly ionized DyII, followed by the generation of neutral DyI atoms. This chain of events, observed by the fluorescence of corresponding ionic and atomic lines, is reflected in faster effective population time for DyII compared to the effective population time of neutral DyI. We note that a very good fit of both, ionic and atomic fluorescence data (see Fig. 5), also indicates that our two-state model for the decay of dysprosium plasma is basically correct. In the case that the cascade involves three or even more states, the experimental data would have much slower fall-off, and the correct fitting function would be a more complicated one (a sum of three or more exponentials). Thus, a very good two-exponential fitting function confirms our model of plasma evolution.

The evolution of plasma temperature and electron density can be followed by monitoring the atomic line widths. However, the measured line widths are broadened by the instrumental profile of our monochromator, and must be deconvoluted. In Fig. 8, we show an enlarged view of the DyI resonance line at 404.597 nm (the section taken from Fig. 2). The open circles represent the measured data, and the full line is the result of a multicomponent fit consisting of eight Gaussian profiles (corresponding to the eight well separated spectral lines shown in Fig. 2). In the fitting procedure, the program varied the peak line intensity and the line width in order to obtain the best nonlinear least-squares curve fit characterized by the minimum of the χ^2-test value. The line positions were kept constant,

as determined by literature data for indicated atomic and ionic lines [16]. The spectral line profile
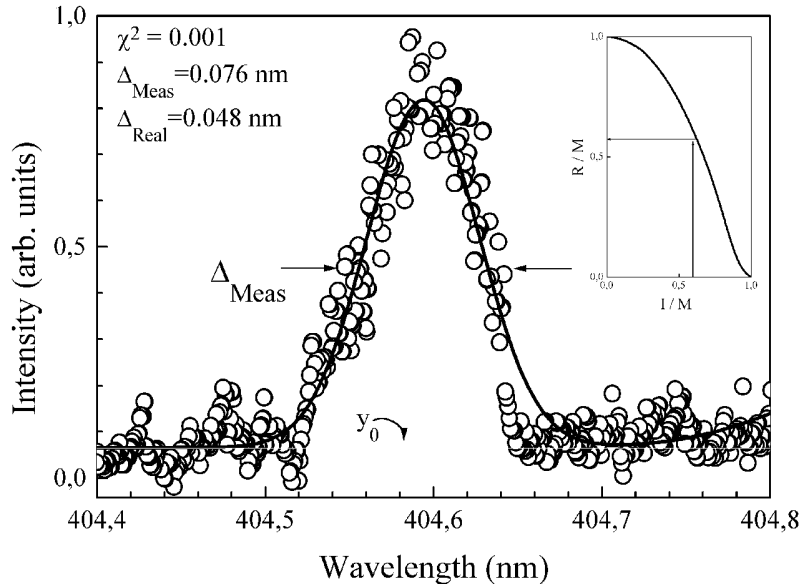

Fig. 8. *Section of plasma plume spectrum at 404.6* nm *showing the details of the* DyI *resonance line shape and the fitting curve approximating the convolution profile. The inset illustrates the procedure for the determination of the real line width by numerical deconvolution.*

shown in Fig. 8 is a convolution of the triangular instrumental profile and the real line profile determined by Stark broadening (a Lorentzian profile [17]). The fit shown in Fig. 8 demonstrates that a Gaussian profile represents an excellent approximation for the exact convolution of a triangular and a Lorentzian profile. The very low value of the χ^2 (the value of 0.001 is typical for all processed spectra) shows that this approximation is the appropriate one. The numerical deconvolution of the experimental data has been performed using this approximation, and the inset in Fig. 8 illustrates the deconvolution procedure. First, we constructed the graph linking the ratios of the I/M (instrumental profile width/measured line width) versus R/M (real line width/measured line width). Knowing this functional relationship, each line width obtained in the fitting procedure can be numerically deconvoluted to obtain the real (Lorentzian) line width. In Fig. 9, we show the results of this procedure applied to the atomic line DyI 404.597 nm (the time dependence of its real line width). The line widths are given versus the box-car gate delay after the laser pulse. The best fit obtained is a simple exponential curve showing a pure exponential decay of Dy plasmas. When the dysprosium plume has been produced in argon, an additional broadening of all spectral lines has been observed. For example, argon pressure of about 20 mbar broadens dysprosium resonance line by about 20%. Unfortunately, the dependence of the DyI linewidth on the electron density and temperature were neither measured nor calculated

until now, and our data can not supply the absolute values for these quantities. We plan to determine the plasma temperature and electron density, and to calibrate our relative linewidth data in a new ablation experiment using a dysprosium pellet containing the Cu and Al atoms as impurities. The broadening of atomic lines of these two elements is well documented, and will serve as a calibration tool for the broadening of Dy spectral lines [19].
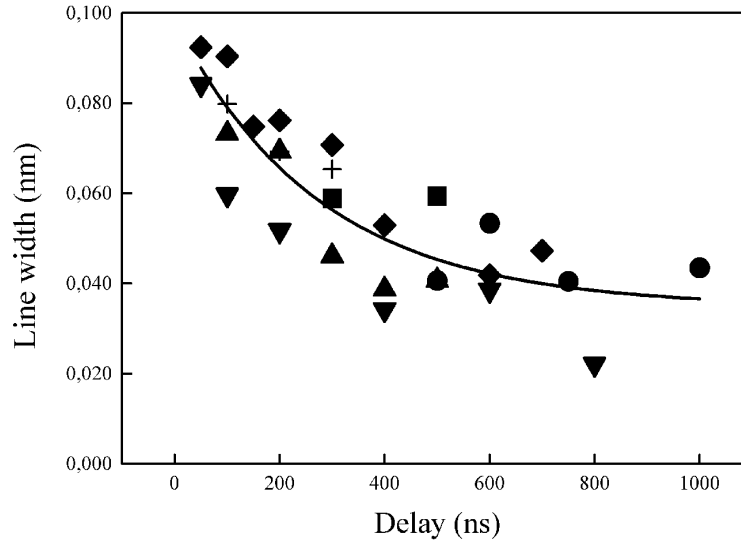

Fig. 9. Time development of the DyI *resonance line width showing an exponential decay of dysprosium plasmas. The exponential growth of the line width for small delays suggests a very hot plasma at the beginning of laser pulse.*

We studied the influence of argon backing gas on the impurity lines of holmium and yttrium appearing in the vicinity of dysprosium lines (see Fig. 2). Generally, the presence of argon enhances impurity lines, too. Under our experimental conditions, maximum of the impurity fluorescence is reached at about 40 mbar Ar pressure. The effect of argon on the line widths is similar, showing an additional line broadening when rising argon pressure. The broadening effect for the impurity lines could not be determined accurately because of the low signal to noise ratio.

4. Conclusion

In our experiment, a standard excimer laser with a pulse duration of about 20 ns has been used. Therefore, the absorption of the laser energy in the sample, the ablation process and the plasma formation all happen essentially at the same time (during the laser pulse) and the role of each process can not be clearly identified. However, this is the case encountered in many similar experiments on laser ablation, and it was appropriate for the purposes of our experiment. We measured energy threshold for dysprosium plasma formation, the

time evolution of DyI and DyII resonance line intensities, the time dependence of neutral DyI line-widths, and the influence of argon backing gas. The analysis of the experimental data gives the time-dependence of the atomic and ionic resonance line widths, and an insight into the dynamics of of laser-induced plasmas. The comparison of the measurements made in vacuum and in argon shows a certain influence of backing gas in the range of 10 – 100 mbar Ar.

Acknowledgements

References

1) D. Budker, D. DeMille, E. D. Commins and M. S. Zolotorev, Phys. Rev. Lett. **70** (1993) 3019;

2) B. Jonson, Physica Scripta **T59** (1995) 53;

3) N. P. Penkin and V. A. Komarovski, JQSRT **16**, (1976) 217;

4) W. P. Moskowitz and W. M. Keeffe, *Proceedings of the 6th International Symposium on the Science and Technology of Light Sources,* (Budapest 1992) 71P; and KE Brown, L Cifuentes, DAJ Mottram SA Mucklejohn and B. Preston, *Proceedings of the 6th International Symposium on the Science and Technology of Light Sources,* (Budapest 1992) p. 56;

5) J. R. Fuhr and A. Lesage: *Bibliography on Atomic Line Shapes and Shifts* (US DoC/NIST Special Publication 366, Gaithersburg 1993);

6) J. Kusz, Astron.Astrophys.(Suppl.) **92** (1992) 517;

7) D. Budker, D. DeMille, E. D. Commins and M. S. Zolotorev, Opt. Lett. **16** (1991) 1514;

8) R. J. Lipert and S. C. Lee, Appl. Phys. **B57** (1993) 373;

9) N. Spector, J. Sugar and J.-F. Wyart, private communication by J. Sugar;

10) RCA Review **30** (1969) 285;

11) D. Budker, D. DeMille, E. D. Commins and M. S. Zolotorev, Phys. Rev. **A50** (1994) 132;

12) P. Hannaford, Opt. Lett. **17** (1992) 432;

13) M. Beau, "Osram A.G.", R&D Labs, private communication;

14) S. Gogić and S. Milosević, in *Spectral Line and Shapes, Vol. 9*, eds. M. Zoppi and L. Ulivi, AIP Conf. Proc. **386**, New York, 1997, p. 163;

15) "Fluka A.G.", Switzerland (1986) Batch #44640/Zert. #1178;

16) W. L. Wiese, and G. A. Martin, *Wavelengths and Transition Probabilities for Atoms and Atomic Ions* (NBS Stand.Ref.Dat.Ser.#68, Gaithersburg 1980);

17) I. I. Sobelman, *Introduction to the Theory of Atomic Spectra* (Oxford:Pergamon 1973);

18) R. W. Dreyfus, J. Appl. Phys. **69** (1990) 1721;

19) H. R. Griem, *Spectral Line Broadening by Plasmas* (Academic Press 1974).

SPEKTROSKOPSKO PROUČAVANJE LASEROM IZAZVANE DISPROZIJEVE PLAZME

Opisuje se proučavanje laserom stvorene disprozijeve plazme. Istražvala se vremenska ovisnost jakosti i širina izabranih rezonantnih linija DyI i DyII. Opazili smo da na vremen-ski razvoj plazme jako utječe prisutnost argona. Usporedba širina linija DyI izmjerenih u vakuumu i u argonu pokazuje malen utjecaj na mjerene Starkove širine linija.